Gold, Palladium, and Gold–Palladium Alloy Nanoshells on Silica Nanoparticle Cores

Jun-Hyun Kim, William W. Bryan, Hae-Won Chung, Chan Young Park, Allan J. Jacobson, and T. Randall Lee*

Department of Chemistry and Texas Center for Superconductivity, University of Houston, 4800 Calhoun Road, Houston, Texas 77204-5003

ABSTRACT The synthesis of gold, palladium, and gold–palladium alloy nanoshells (~15–20 nm thickness) was accomplished by the reduction of gold and palladium ions onto dielectric silica core particles (~100 nm in diameter) seeded with small gold nanoparticles (~2–3 nm in diameter). The size, morphology, elemental composition, and optical properties of the nanoshells were characterized using field-emission scanning electron microscopy, transmission electron microscopy, energy-dispersive X-ray spectroscopy, X-ray diffraction, and ultraviolet–visible spectroscopy. The results demonstrate the successful growth of gold, palladium, and gold–palladium alloy nanoshells, where the optical properties systematically vary with the relative content of gold and palladium. The alloy nanoshells are being prepared for use in applications that stand to benefit from photoenhanced catalysis.

KEYWORDS: gold • palladium • alloy • metal • nanoshells • nanoparticles

INTRODUCTION

Environmental concerns and increasing demands for renewable energy have prompted the development of new nanoscale materials that utilize solar energy. Nanoscale materials are attractive targets because, due to their large surface-to-volume ratio, they exhibit properties that can be significantly different from those of bulk materials (1). To this end, scientists have been synthesizing a variety of metal nanoparticles with the goal of generating new types of nanoscale materials for use in photocatalytic applications (2–5). Metal nanoparticles composed of gold, silver, palladium, or copper have unique optical properties arising from their surface plasmon resonance; their sometimes unanticipated catalytic properties warrant further investigation (6, 7). The systematic design and modification of such metal nanoparticles remains, however, a challenging objective (8, 9). For example, existing "dry" physical synthetic methods often require high-temperature evaporation or laser ablation of bulk metal precursors (4, 10, 11), both of which are costly and require specialized equipment. In contrast, "wet" chemical synthetic methods typically involve the reduction of metal ions in solution (12, 13), which is a relatively inexpensive and technologically simple approach.

The study and use of metal nanoparticles comprised of two or more metallic elements has drawn much attention because of the potential for combining and exploiting the attractive properties of each metal (14–16). In a specific example, Toshima and co-workers showed that gold–palladium alloy nanoparticles were more active in catalyzing the hydrogenation of 1,3-cyclooctadiene than were nanoparticles derived solely from either gold or palladium (17, 18). The authors concluded that the high catalytic activity of the bimetallic system arose from the change in the electron density on the surface due to the differing ionization potentials of gold and palladium. Similarly, Mou and co-workers showed that gold–silver alloy nanoparticles were more active in catalyzing CO oxidation than were nanoparticles derived solely from either gold or silver (19). Thus, the development of new alloy nanoparticles offers unique reactivity when compared to monometallic nanoparticles.

The reduction of hydrogen tetrachloroaurate(III) readily affords gold nanoparticles, but the plasmon resonance of these nanoparticles is typically limited to a narrow range of wavelengths (i.e., 540 ± 20 nm) (20). However, with the recent development of gold shell–dielectric core structures prepared by seeded-growth methods (9, 21–23), the plasmon resonance can be tuned from visible to near-IR wavelengths (i.e., across nearly the entire solar spectrum that reaches the surface of the earth) (24), by judiciously varying the shell thickness and/or core size. These metal nanoshells have the potential for use in many technologies, ranging from light-emitting devices to biosensing and drug-delivery applications (25–27). Furthermore, the incorporation of catalytic function into these core–shell structures (e.g., the addition of highly catalytically active palladium) allows for the formation of nanoscale materials that can be used as photoactivated and/or photoenhanced catalysts. With regard to the latter applications, the absorption of light by alloy nanoshells at wavelengths ranging from the ultraviolet to the near-IR will lead to rapid and efficient heating of the surface of the nanoparticle (28). This photoderived heating may be used to initiate and/or enhance the catalytic activity of the alloy.

Several synthetic routes for the preparation of nanoscale materials with photocatalytic properties have been developed, with much attention focused on TiO_2 nanocomposites (4, 29, 30). In contrast, our approach seeks to couple the

* To whom correspondence should be addressed. E-mail:trlee@uh.edu.
Received for review January 19, 2009 and accepted April 2, 2009

DOI: 10.1021/am900039a

strong optical absorbances of gold nanoshells with the excellent catalytic properties of palladium nanoparticles through the preparation and utilization of gold−palladium alloy nanoshells. Palladium nanoparticles have been used to catalyze a variety of organic transformations, including the hydrogenation of olefins and dienes (31), the hydration of acrylonitrile to acrylamide (32), the photogeneration of hydrogen from water (33), and the reduction of carbon dioxide (34). While the majority of research efforts have focused on catalysis by single-component palladium nanoparticles, studies of catalysis by nanoparticle alloys of palladium (e.g., bimetallics and trimetallics) have also enjoyed a rich history (35), although we have found no reports of the use of shell−core nanoparticle architectures for such photocatalytic applications.

In the present report, we describe the simultaneous chemical reduction of gold and palladium salts in the presence of gold-seeded silica core nanoparticles to afford a series of gold−palladium alloy nanoshells (∼15−20 nm thickness) on the silica cores (∼100 nm in diameter). Using this wet chemical approach, which allows facile control over both the ratio of gold−palladium and the dimensions of the particles (22, 36), we also prepare analogous single-component gold and palladium nanoshells for comparison. We thoroughly characterize these shell−core nanoparticles using field-emission scanning electron microscopy (FE-SEM), transmission electron microscopy (TEM), energy-dispersive X-ray spectroscopy (EDX), X-ray diffraction (XRD), and ultraviolet−visible (UV−vis) spectroscopy. Finally, we discuss the potential benefits of particular gold−palladium alloy nanoshell compositions whose optical properties render them attractive for use in photocatalytic applications, which will be explored in studies subsequent to this initial investigation.

EXPERIMENTAL SECTION

Materials. Ammonium hydroxide (30% NH_3), nitric acid, hydrochloric acid (all from EM Science), tetraethylorthosilicate, tetrakis(hydroxymethyl)phosphonium chloride (THPC), (3-aminopropyl)trimethoxysilane (APTMS) (all from Aldrich), hydrogen tetrachloroaurate(III) hydrate (Strem), ethanol (McKormick Distilling Co.), potassium carbonate (J. T. Baker), palladium(II) chloride (Acros), and L-ascorbic acid sodium salt (Chemalog) were used without modification from the indicated commercial suppliers. Deionized water was purified to a resistance of 18 MΩ (Academic Milli-Q Water System; Millipore Corp.) and filtered through a 0.22 μm membrane filter. All glassware was cleaned using an aqua regia solution (3:1 HCl−HNO_3), followed by treatment in a base bath (saturated KOH in isopropyl alcohol), and then rinsing with Milli-Q water prior to use.

Attachment of THPC Gold Seeds to Amine-Functionalized Silica Particles. Silica core nanoparticles (∼100 nm in diameter) functionalized with APTMS have been described elsewhere (37−39). Samples of these nanoparticles were centrifuged at 3000 rpm for 1 h using a RC-3B refrigerated centrifuge (Sorvall Instruments). The particles were redispersed three times in 100 mL of absolute ethanol to remove unattached APTMS molecules, small silica nanoparticle contaminants, and any other side products.

To attach THPC-reduced gold seeds to the silica nanoparticles, we used a self-assembly method developed by Westcott et al. (40). The gold seeds were prepared by the reduction of a 1% aqueous solution of $HAuCl_4$ with THPC according the method of Duff and Baiker (41). The resulting gold solution was stored at 4 °C for 3 days before further use. THPC gold nanoparticles (50 mL) were then mixed with an aliquot of the amine-functionalized silica nanoparticles (1 mL) and shaken for 2−3 min. The mixture was allowed to sit for at least 12 h at room temperature to form THPC gold seeds on silica particles by self-assembly. The final mixture was centrifuged for 1 h at 3000 rpm to precipitate the THPC gold-seeded silica particles. The dark-red precipitate was redispersed in 50 mL of Milli-Q water, sonicated for 2−3 min, and centrifuged at 3000 rpm for 1 h. The final solution containing THPC gold-seeded silica particles was light red in color after the precipitates were redispersed in 50 mL of Milli-Q water. Using TEM, we found that the THPC gold seeds had diameters of ∼1−3 nm and the silica particles had diameters of ∼100 nm.

Gold, Palladium, and Gold−Palladium Alloy Nanoshell Growth. The targeted metal shells were grown on silica nanoparticle cores using a combination of nanoparticle−synthesis methods reported in the literature (21, 36, 40, 42). A 0.5 mM solution of palladium chloride was prepared by dissolving 0.01773 g of $PdCl_2$ in a mixture of 196 mL of water and 4 mL of a 50 mM HCl solution. A 0.5 mM gold stock solution was prepared by mixing 2 mL of an aqueous 1% $HAuCl_4$ solution and 0.025 g of potassium carbonate (K_2CO_3) in 100 mL of water. A series of 10 mL aliquots were placed in 25 mL beakers equipped with magnetic stirring bars, where the ratio (mL) of palladium:gold was systematically varied: (a) 0:10, (b) 2:8, (c) 4:6, (d) 5:5, (e) 6:4, (f) 8:2, and (g) 10:0. We then added 2 mL of prepared THPC gold seeds on silica particles to each of the 10 mL reaction mixtures. The final solutions were thoroughly stirred for at least 10 min, and then 0.6 mL of L-ascorbic acid (100 mM) was added quickly to reduce the palladium and gold salts simultaneously onto the THPC gold-seeded silica core particles. The color changed from yellow to green, blue, or dark steel blue, depending on the palladium:gold ratio. All of the samples were centrifuged at 3000 rpm for 30 min and redispersed in Milli-Q water at least twice to remove unreacted chemicals or detached-seed particles during the growth process. Samples were preserved in the refrigerator before characterization.

Characterization Methods. To analyze the size distribution, coarse morphology, and elemental composition of the nanoshells, we used a JEOL JSM 6330F FE-SEM instrument operating at 15 kV equipped with an EDX instrument (Link ISIS software series 300, Oxford Instruments). All samples were deposited from solution onto holey carbon-coated copper grids and completely dried at room temperature at least 12 h prior to sputter-coating with carbon (i.e., samples were coated with ∼25 nm of carbon via sputtering to improve the electrical conductivity for imaging). EDX analyses of the bare holey carbon-coated copper grids were also performed to rule out the possibility of contamination.

We employed TEM to obtain images of the shell−core structures, which allowed a detailed analysis of the particle morphologies. The images were collected using a JEOL JEM-2000 FX transmission electron microscope operating at a bias voltage of 200 kV. Sample preparation involved the deposition of an aqueous solution of alloy nanoshells onto a 300-mesh holey carbon-coated copper grid. As described above, the samples were allowed to dry thoroughly before analysis.

We used a powder X-ray diffractometer (Scintag XDS 2000) with monochromatic Cu Kα radiation ($\lambda = 1.540\,562$ Å) and a step width of 0.02° to analyze the structural and compositional features of the various nanoshells. The samples subjected to XRD analysis were prepared by centrifuging the gold, palladium, and gold−palladium alloy (1:1) nanoshells, depositing the concentrated solution of nanoshells on a quartz glass substrate, and drying the samples under vacuum at 30 °C overnight.

To characterize the optical properties of the nanoshells, we collected UV−vis spectra over the wavelength range of 200−1100

nm using a Cary 50 Scan UV−vis spectrometer. All samples were prepared by centrifugation of the nanoshell solution at least twice, followed by redispersement in water and transfer to a quartz UV−vis cell.

RESULTS AND DISCUSSION

We adopted a seeded-growth method to prepare gold, palladium, and gold−palladium alloy nanoshells (~15−20 nm thick) on dielectric silica cores (~100 nm diameter), where small THPC gold seeds (~2 nm diameter) were attached to the silica core particles and allowed to serve as nucleation sites for shell growth. This approach is known to afford monodisperse nanoshells that are colloidally stable in an aqueous solution (21). Furthermore, based on the results from previous reports (21, 23, 36, 43, 44), we believed that use of the seeded-growth method would allow ready control over shell thicknesses and composition. Our strategy employed the known reducing agent L-ascorbic acid to effect the growth of the nanoshells (22, 36).

Figure 1 shows FE-SEM images of THPC gold-seeded silica cores and a series of nanoshells having systematically varying compositions of gold and palladium. From the FE-SEM images and dynamic light scattering measurements, the silica core nanoparticles are all monodisperse and consistently ~100 nm in diameter; similarly, all of the nanoshells are ~130−140 nm in diameter. While the THPC gold-seeded silica nanoparticles are monodisperse with smooth surfaces, the nanoshells appear to have markedly rougher surfaces, particularly for the nanoshells with low ratios of palladium:gold. We note also that many of the nanoshells imaged by FE-SEM and shown in Figure 1 appear to exhibit shell−core morphologies (e.g., images b, c, e, and f), while other nanoshells exhibit no such features (e.g., images d, g, and h). As such, we sought a more definitive structural characterization of the nanoshells through the use of TEM.

Analysis of the nanoshells by TEM confirms, first of all, their relatively rough morphology (see Figure 2), which is likely a consequence of the reducing agent used; we note that the use of formaldehyde as the reducing agent typically affords gold nanoshells with markedly smoother surface morphologies than those shown here (21, 44). As suggested by the FE-SEM images, the nanoshell surfaces become smoother and more homogeneous with increasing ratios of palladium:gold; apparently, L-ascorbic acid is a preferred reducing agent for palladium (22, 36), while formaldehyde is a preferred reducing agent for gold (21, 44). Importantly, the images in Figure 2 are consistent with complete shell formation (21). Moreover, when compared to TEM images of the silica core particle templates (not shown), the TEM images in Figure 2 indicate shell thicknesses of ~15−20 nm for all compositions, which is consistent with FE-SEM images.

We used analysis by EDX to evaluate the elemental composition of the nanoshells. A typical spectrum is shown in Figure 3, where we used a 50:50 ratio of palladium:gold salts in the synthesis of the nanoshells. Figure 3 shows a peak characteristic of palladium (Lα, Lβ) at 2.85 keV and peaks characteristic of gold (Mα, Lα) at 2.12 and 9.71 keV, as well as a small peak from silicon (Kα, Kβ) at 1.75 keV and a small peak from copper (Kα) at 8.04 keV, which can be attributed to the sample grid. The presence of intense peaks for palladium and gold indicates possible alloy nanoshell formation in the shell, while the presence of a weak peak for silicon is consistent with this element residing underneath a thin gold−palladium shell. Because EDX can detect core elements at sampling depths of ≤2 μm (45), the observation of silicon in the EDX spectra of nanoshells is plausible even with complete shell formation. We note further that previous studies using X-ray photoelectron spectroscopy demonstrated similar growth of defect-free gold shells on silica nanoparticle cores (21), and separate studies demonstrated the reliable formation of gold−palladium alloy (or bimetallic) nanoparticles via the co-reduction of gold and palladium salts (17, 18, 46−48). Studies of the latter alloy nanoparticles found that palladium atoms tended to concentrate on the surface of the nanoparticles and gold atoms tended to concentrate in the cores because of the different rates of reduction of the respective metal ions (i.e., gold ions undergo reduction more readily than palladium ions) (17, 48).

Table 1 shows the atomic percentages of gold and palladium obtained by EDX analysis of the series of nanoshells, confirming that the final compositions of the nanoshells closely match the relative metal salt concentrations used in the synthetic preparations (49). Interestingly, the nanoshells prepared without using $HAuCl_4$ were, nevertheless, observed to contain ~2% gold, which probably arises from the presence of the initial THPC gold seeds. In most other cases, the content of palladium appears to be slightly enhanced, particularly for nanoshells having low contents of palladium. This apparent enhancement might, however, arise from the aforementioned tendency of palladium to concentrate at the surfaces of the nanoparticles (17, 48), existing in part as thin palladium layers covering a gold-enriched core (21, 50). Recent detailed work by the groups of Crooks (50) and Rodriguez (51) using extended X-ray absorption fine structure spectroscopy explored this phenomenon in samples of relatively small alloy nanoparticles (typically <10 nm), where the particles were shown unambiguously to possess a gold-rich core surrounded by a palladium-rich shell. Nevertheless, the EDX analyses in Table 1 of our markedly larger mixed-metal-coated nanoparticles are consistent with the formation of gold−palladium alloy nanoshells on silica nanoparticle cores.

To verify the formation of gold−palladium alloy nanoshells, we analyzed selected samples of nanoshells using XRD (see Figure 4). The broad band at ~20−30° corresponds to the sample holder due to difficulties in preparing smooth and well-packed samples. The pure gold nanoshells exhibit XRD peaks at 38.2°, 44.4°, and 64.8° corresponding to the (111), (200), and (220) planes, respectively, of the face-centered-cubic (fcc) structure of gold with space group *Fm*3*m* (JCPDS Card No. 4-784). Similarly, the pure palladium nanoshells exhibit XRD peaks at 39.8°, 46.2°, and 67.5° corresponding to the (111), (200), and (220) planes, respectively, of the fcc structure of palladium with space group *Fm*3*m* (JCPDS Card

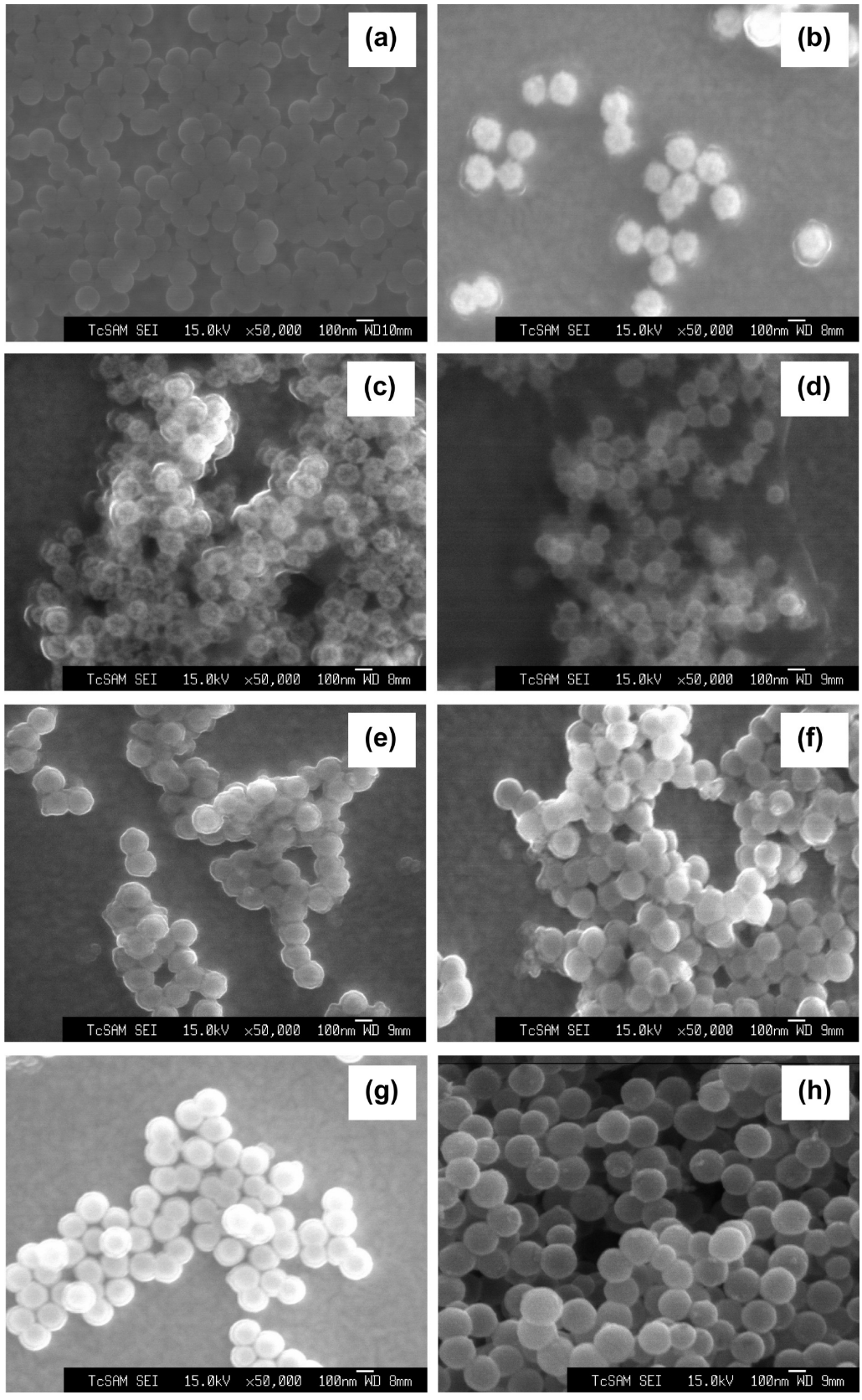

FIGURE 1. FE-SEM images of (a) THPC gold seeds on silica cores and gold, palladium, and gold–palladium alloy nanoshells, where the ratio of palladium:gold was systematically varied: (b) 0:100, (c) 20:80, (d) 40:60, (e) 50:50, (f) 60:40, (g) 80:20, (h) 100:0.

No. 46-1043). Importantly, the sample containing discrete gold nanoshells mixed with discrete palladium nanoshells (1:1 Au + Pd mixture) exhibits six distinctive peaks: three peaks from gold and three peaks from palladium. In contrast, the 50:50 gold–palladium bimetallic nanoshells exhibit three distinctive peaks at 38.7°, 44.9°, and 65.9° related

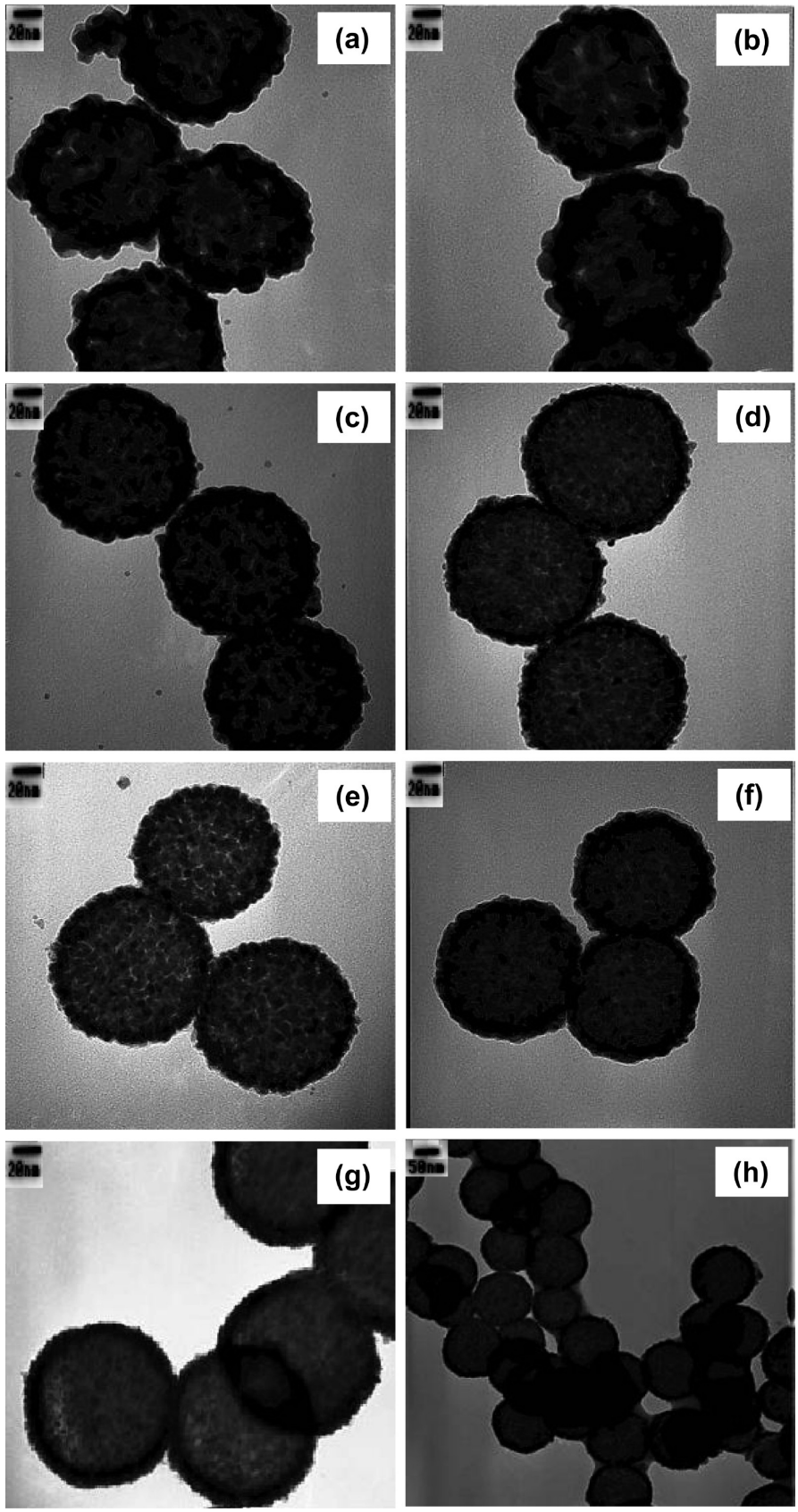

FIGURE 2. TEM images of gold, palladium, and gold–palladium alloy nanoshells, where the ratio of palladium:gold was systematically varied: (a) 0:100, (b) 20:80, (c) 40:60, (d) 50:50, (e) 60:40, (f) 80:20, (g) 100:0. Image h shows the general distribution for a sample of pure palladium nanoshells (i.e., Pd:Au = 100:0).

to the peak positions of the (111), (200), and (220) planes, respectively. These results are consistent with previous XRD studies of gold–palladium alloy nanoparticles in which the XRD peaks were found to lie between those of pure gold and

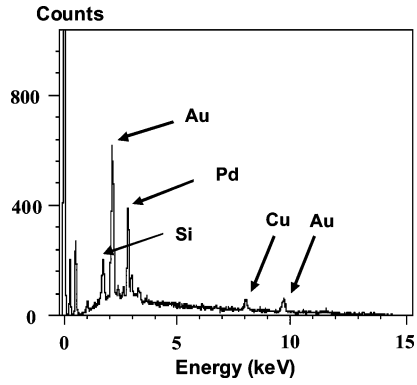

FIGURE 3. EDX spectrum of gold–palladium alloy nanoshells (Pd:Au = 50:50).

Table 1. Nanoshell Atomic Compositions Obtained by EDX Analysis†

initial mole %		atomic %	
Pd	Au	Pd	Au
100	0	98 ± 1	2 ± 1
80	20	79 ± 3	21 ± 3
60	40	64 ± 4	36 ± 4
50	50	54 ± 4	46 ± 4
40	60	46 ± 3	54 ± 3
20	80	28 ± 4	72 ± 4
0	100	0	99 ± 1

pure palladium nanoparticles (47). Thus, we conclude that the powder XRD patterns strongly indicate that the co-reduction of mixtures of gold and palladium salts in the presence of gold-seeded silica cores leads to the formation of gold–palladium alloy nanoshell particles.

On the basis of previous studies of related systems (43, 52), we anticipated that the optical properties of the nanoshells could be varied in a controlled manner by adjusting the relative amounts of gold and palladium salt precursors. To this end, Figure 5 shows the UV–vis spectra of the gold, palladium, and gold–palladium alloy nanoshells. Upon

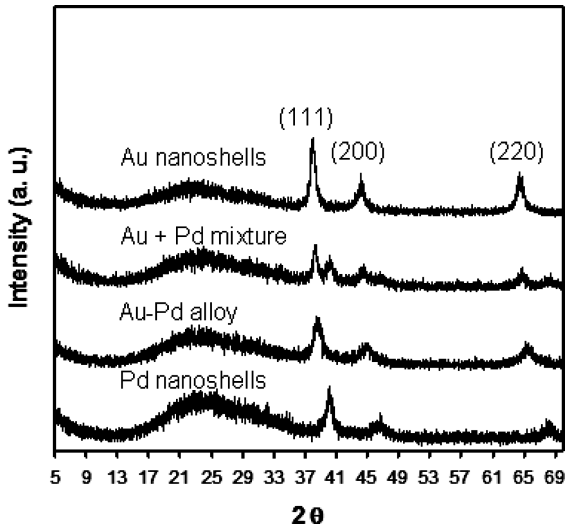

FIGURE 4. XRD patterns of pure gold nanoshells, a 1:1 mixture of pure gold nanoshells and pure palladium nanoshells, gold–palladium alloy nanoshells (Pd:Au = 50:50), and pure palladium nanoshells.

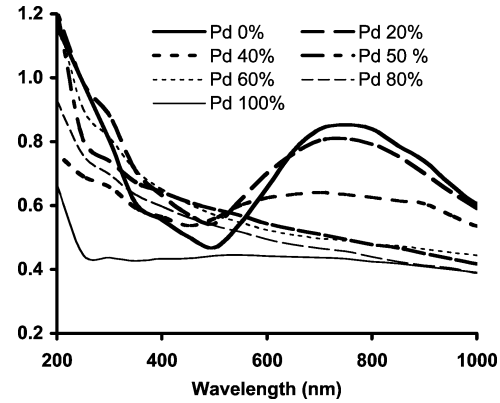

FIGURE 5. UV–vis spectra of gold, palladium, and gold–palladium alloy nanoshells with increasing amounts of palladium.

formation of the nanoshells, the absorptions centered at 235 and 300 nm corresponding to palladium(II) and gold(III) ions completely disappear (46, 53). As predicted by the Mie theory (54), pure gold nanoshells (i.e., with 0% Pd) having ~20 nm thickness show an intense plasmon absorption at ~780 nm, indicating the formation of complete metal shells. Upon introduction of palladium (i.e., 80% Au and 20% Pd), the plasmon absorption resembles that of the pure gold nanoshells, but with lower intensity. Furthermore, as a consequence of increasing the palladium content further (i.e., 60% Au and 40% Pd), the absorption intensity decreases dramatically. Moreover, as the palladium content approaches 100%, the plasmon absorption approaches zero over the wavelengths monitored, which suggests an increasing presence of palladium atoms on the surfaces of the particles (46, 48, 55).

An important conclusion that can be drawn from the absorption spectra in Figure 5 is that the content of palladium in gold–palladium alloy nanoshells should not exceed ~40% in applications where photoenhanced catalysis is desired. Fortunately, precedents exist in which bimetallic gold–palladium catalysts having relatively small contents of palladium exhibit enhanced activity and/or selectivity compared to the corresponding single-component catalysts (48, 56–58). For example, Liu et al. demonstrated the higher catalytic activity of gold–palladium bimetallic nanoparticles compared to those of either gold or palladium monometallic nanoparticles for both the hydrogenation of *cis*-1,3-cyclooctadiene and the hydrogenolysis of *p*-nitrotoluene (48). Furthermore, Wong and co-workers observed enhanced catalytic activity for submonolayer coverages of palladium on gold core nanoparticles in the hydrodehalogenation of trichloroethene (56). Similarly, Lambert and co-workers found that increasing the content of gold on the surface of palladium shell–gold core nanoparticles led to a pronounced selectivity toward the production of benzene versus *n*-hexane in the cyclotrimerization of acetylene (57). Separate studies by Goodman and co-workers found enhanced rates for the acetoxylation of ethylene to give vinyl acetate when catalyzed by submonolayer coverages of palladium on gold single-crystal surfaces (58) or by supported bimetallic nanoparticles in which the atomic ratio of palladium:gold was 4:1 (59). In work that is perhaps more aligned with our ultimate goals, He and co-

workers recently reported the preparation of TiO_2-coupled $NiTiO_3$ nanoparticles having 40−50 nm diameters and the capacity to absorb visible light; moreover, the catalytic degradation of methylene blue by these particles could be effected by irradiation with visible light (60). This nonexhaustive list of examples, when coupled with the encouraging absorption spectra in Figure 5 (i.e., strong optical absorbances that span the wavelengths at which incident solar radiation is most intense on the surface of the earth) (61), argues that future studies of photoenhanced catalysis by gold−palladium alloy nanoshells are warranted.

CONCLUSIONS

This research has demonstrated the preparation of shell−core nanoparticles consisting of gold, palladium, and gold−palladium alloy shells (∼15−20 nm thickness) on silica nanoparticle cores (∼100 nm in diameter) using a modified seeded-growth method with the reduction of metal ions by L-ascorbic acid at room temperature in an aqueous environment. Analysis of the nanoshell particles by FE-SEM, TEM, EDX, XRD, and UV−vis collectively confirms the formation of the targeted metallic nanoshells, including the confirmation by XRD of alloy shell growth. Importantly, spectroscopic measurements show that gold−palladium alloy nanoshells prepared with no more than ∼40% Pd show appreciable absorbances over visible and near-IR wavelengths; in contrast, when the palladium content is raised above ∼40%, the absorbances fall to values near zero. As a whole, the results demonstrate that gold−palladium alloy nanoshells have the potential for use in photoenhanced catalysis.

Acknowledgment. We acknowledge generous financial support from the Army Research Office, the Texas Center for Superconductivity, and the Robert A. Welch Foundation (Grant E-1320). We also thank Dr. I. Rusakova for assistance with the TEM measurements and Dr. J. K. Meen for assistance with the FE-SEM measurements.

REFERENCES AND NOTES

(1) Ye, H.; Scott, R. W. J.; Crooks, R. M. *Langmuir* **2004**, *20*, 2915.
(2) Chen, X.; Zhu, H. Y.; Zhao, J. C.; Zheng, Z. F.; Gao, X. P. *Angew. Chem., Int. Ed.* **2008**, *47*, 5353.
(3) Li, H.; Bian, Z.; Zhu, J.; Huo, Y.; Li, H.; Lu, Y. *J. Am. Chem. Soc.* **2007**, *129*, 4538.
(4) Keskinen, H.; Makela, J. M.; Aromaa, M.; Keskinen, J.; Areva, S.; Teixeira, C. V.; Rosenholm, J. B.; Pore, V.; Ritala, M.; Leskela, M.; Raulio, M.; Salkinoja-Salonen, M. S.; Levanen, E.; Mantyla, T. *Catal. Lett.* **2006**, *111*, 127.
(5) Abe, R.; Takami, H.; Murakami, N.; Ohtani, B. *J. Am. Chem. Soc.* **2008**, *130*, 7780.
(6) Turner, M.; Golovko, V. B.; Vaughan, O. P. H.; Abdulkin, P.; Berenguer-Murcia, A.; Tikhov, M. S.; Johnson, B. F. G.; Lambert, R. M. *Nature (London)* **2008**, *454*, 981.
(7) Bright, R. M.; Musick, M. D.; Natan, M. J. *Langmuir* **1998**, *14*, 5695.
(8) Wu, H.-Y.; Huang, W.-L.; Huang, M. H. *Cryst. Growth Des.* **2007**, *7*, 831.
(9) Jiang, Z.-J.; Liu, C.-Y. *J. Phys. Chem. B* **2003**, *107*, 12411.
(10) Pyatenko, A.; Shimokawa, K.; Yamaguchi, M.; Nishimura, O.; Suzuki, M. *Appl. Phys. A: Mater. Sci. Process.* **2004**, *79*, 803.
(11) Osterwalder, N.; Capello, C.; Hungerbuehler, K.; Stark, W. J. *J. Nanopart. Res.* **2006**, *8*, 1.
(12) Cook, S. C.; Padmos, J. D.; Zhang, P. *J. Chem. Phys.* **2008**, *128*, 154705.
(13) Okitsu, K.; Mizukoshi, Y.; Bandow, H.; Yamamoto, T. A.; Nagara, Y.; Maeda, Y. *J. Phys. Chem. B* **1997**, *101*, 5470.
(14) Ferrando, R.; Jellinek, J.; Johnston, R. L. *Chem. Rev.* **2008**, *108*, 845.
(15) Liu, J. B.; Dong, W.; Zhan, P.; Wang, S. Z.; Zhang, J. H.; Wang, Z. L. *Langmuir* **2005**, *21*, 1683.
(16) Zhang, J.; Liu, H.; Wang, Z.; Ming, N. *J. Solid State Chem.* **2007**, *180*, 1291.
(17) Toshima, N.; Harada, M.; Yamazaki, Y.; Asakura, K. *J. Phys. Chem.* **1992**, *96*, 9927.
(18) Harada, M.; Asakura, K.; Toshima, N. *J. Phys. Chem.* **1993**, *97*, 5103.
(19) Liu, J.-H.; Wang, A.-Q.; Chi, Y.-S.; Lin, H.-P.; Mou, C.-Y. *J. Phys. Chem. B* **2005**, *109*, 40.
(20) Link, S.; Wang, Z. L.; El-Sayed, M. A. *J. Phys. Chem. B* **1999**, *103*, 3529.
(21) Pham, T.; Jackson, J. B.; Halas, N. J.; Lee, T. R. *Langmuir* **2002**, *18*, 4915.
(22) Lu, L.; Wang, H.; Xi, S.; Zhang, H. *J. Mater. Chem.* **2002**, *12*, 156.
(23) Kim, J.-H.; Lee, T. R. *J. Biomed. Pharm. Eng.* **2008**, *2*, 29.
(24) Zhu, J. *Appl. Opt.* **2008**, *47*, 5848.
(25) Hale, G. D.; Jackson, J. B.; Shmakova, O. E.; Lee, T. R.; Halas, N. J. *Appl. Phys. Lett.* **2001**, *78*, 1502.
(26) Khlebstov, B. N.; Khlebstov, N. G. *J. Quant. Spectrosc. Radiat. Transfer* **2007**, *106*, 154.
(27) Kim, J.-H.; Lee, T. R. *Drug Dev. Res.* **2006**, *67*, 61.
(28) Elliot, A. M.; Hazle, J. D.; Li, C.; Stafford, R. J. *Proc. SPIE* **2008**, *6865*, 68650O.
(29) Cho, J.; Denes, F. S.; Timmons, R. B. *Chem. Mater.* **2006**, *18*, 2989.
(30) Shanmugam, S.; Gabashvili, A.; Jacob, D. S.; Yu, J. C.; Gedanken, A. *Chem. Mater.* **2006**, *18*, 2275.
(31) Hirai, H.; Toshima, N. In *Tailored Metal Catalysts*; Iwasawa, Y., Ed.; Reidel Publishing: Dordrecht, Holland, 1986.
(32) Toshima, N.; Wang, Y. *Adv. Mater.* **1994**, *6*, 245.
(33) Bard, A. J. *Science* **1980**, *207*, 139.
(34) Mandler, D.; Willner, I. *J. Am. Chem. Soc.* **1987**, *109*, 7884.
(35) Coq, B.; Figueras, F. *J. Mol. Catal. A: Chem.* **2001**, *173*, 117.
(36) Kim, J.-H.; Chung, H. W.; Lee, T. R. *Chem. Mater.* **2006**, *18*, 4115.
(37) Stober, W.; Fink, A.; Bohn, E. *J. Colloid Interface Sci.* **1968**, *26*, 62.
(38) Waddell, T. G.; Leyden, D. E.; DeBello, M. T. *J. Am. Chem. Soc.* **1981**, *103*, 5303.
(39) van Blaaderen, A.; Vrij, A. J. *J. Colloid Interface Sci.* **1993**, *156*, 1.
(40) Westcott, S. L.; Oldenburg, S. J.; Lee, T. R.; Halas, N. J. *Langmuir* **1998**, *14*, 5396.
(41) Duff, D. G.; Baiker, A. *Langmuir* **1993**, *9*, 2301.
(42) Kim, S.-W.; Kim, M.; Lee, W. Y.; Hyeon, T. *J. Am. Chem. Soc.* **2002**, *124*, 7642.
(43) Kim, J.-H.; Bryan, W. B.; Lee, T. R. *Langmuir* **2008**, *24*, 11147.
(44) Kim, J.-H.; Lee, T. R. *Proc. Int. Conf. Biomed. Pharm. Eng.* **2006**, *1*, 271.
(45) Laskin, A.; Cowin, J. P. *Anal. Chem.* **2001**, *73*, 1023.
(46) Mizukoshi, Y.; Okitsu, K.; Maeda, Y.; Yamamoto, T. A.; Oshima, R.; Nagata, Y. *J. Phys. Chem. B* **1997**, *101*, 7033.
(47) Sanchez-Ramirez, J. F.; Pal, U. *Superficies Vacio* **2001**, *13*, 114.
(48) Liu, H.; Mao, G.; Meng, S. *J. Mol. Catal.* **1992**, *74*, 275.
(49) Wu, M.-L.; Chen, D.-H.; Huang, T. C. *Langmuir* **2001**, *17*, 3877.
(50) Knecht, M. R.; Weir, M. G.; Frenkel, A. I.; Crooks, R. M. *Chem. Mater.* **2008**, *20*, 1019.
(51) Teng, X.; Wang, Q.; Liu, P.; Han, W.; Frenkel, A. I.; Wen, W.; Marinkovic, N.; Hanson, J. C.; Rodriguez, J. A. *J. Am. Chem. Soc.* **2008**, *130*, 1093.
(52) Mulvaney, P.; Giersig, M.; Henglein, A. *J. Phys. Chem.* **1992**, *96*, 10419.
(53) Teranishi, T.; Miyake, M. *Chem. Mater.* **1998**, *10*, 594.
(54) Mie, G. *Ann. Phys.* **1908**, *25*, 377.
(55) Nath, S.; Praharaj, S.; Panigrahi, S.; Ghosh, S. K.; Kundu, S.; Basu, S.; Pal, T. *Langmuir* **2005**, *21*, 10405.
(56) Nutt, M. O.; Hughes, J. B.; Wong, M. S. *Environ. Sci. Technol.* **2005**, *39*, 1346.
(57) Lee, A. F.; Baddeley, C. J.; Hardacre, C.; Ormerod, R. M.; Lambert, R. M.; Schmid, G.; West, H. *J. Phys. Chem.* **1995**, *99*, 6096.
(58) Han, Y.-F.; Wang, J.-H.; Kumar, D.; Yan, Z.; Goodman, D. W. *J. Catal.* **2005**, *232*, 467.
(59) Chen, M.; Kumar, D.; Yi, C.-W.; Goodman, D. W. *Science* **2005**, *310*, 291.
(60) Shu, X.; He, J.; Chen, D. *Ind. Eng. Chem. Res.* **2008**, *47*, 4750.
(61) Gueymard, C.; Myers, D.; Emery, K. *Sol. Energy* **2002**, *73*, 443.

AM900039A